Consistent Linear-Elastic Transformations for Image Matching

Gary E. Christensen

Department of Electrical and Computer Engineering
The University of Iowa, Iowa City, Iowa 52242, USA
gary-christensen@uiowa.edu

Abstract. A fundamental problem with a large class of image registration techniques is that the estimated transformation from image A to B does not equal the inverse of the estimated transform from B to A. This inconsistency is a result of the matching criteria's inability to uniquely describe the correspondences between two images. This paper seeks to overcome this limitation by jointly estimating the transformation from A to B and from B to A while enforcing the consistency constraint that these transforms are inverses of one another. The transformations are further restricted to preserve topology by constraining them to obey the laws of continuum mechanics. A new parameterization of the transformation based on a Fourier series in the context of linear elasticity is presented. Results are presented using both Magnetic Resonance and X-ray Computed Tomography Imagery. It is shown that joint estimation of a consistent set of forward and reverse transformations constrained by linear-elasticity gives better registration results than using either constraint alone or none at all.

1 Introduction

A reasonable but perhaps not always desirable assumption is that the mapping of one anatomical image (source) to another (target) is diffeomorphic, i.e., continuous, one-to-one, onto, and differentiable. By definition, a diffeomorphic mapping has an unique inverse that maps the target image back onto the source image. Thus, it is reasonable goal to estimate a transformation from image A to B that should equal the inverse of the transformation estimated from B to A assuming a diffeomorphic mapping exists between the images. However, this consistency between the forward and reverse transformations is not guaranteed with many image registration techniques.

Depending on the application, the diffeomorphic assumption may or may not be valid. This assumption is valid for registering images collected from the same individual imaged by two different modalities such as MRI and CT, but it is not necessarily valid when registering images before and after surgery. Likewise, a diffeomorphic mapping assumption may be valid for registering MRI data from two different normal individuals if the goal is to match the deep nuclei of the

A. Kuba et al. (Eds.): IPMI'99, LNCS 1613, pp. 224–237, 1999.

brain, but it may not be valid for the same data sets if the goal is to match the sulcal patterns.

Alternatively, diffeomorphic transformations may be used to identify areas where two image volumes differ topologically by analyzing the properties of the resulting transformation. For example, consider the problem of matching an MRI image with a tumor to one without a tumor. A possibly valid diffeomorphic transformation would be one that registers all of the corresponding brain structures by shrinking the tumor to a small point. Such a transformation would have an unusually small Jacobian which could be used to detect or identify the location of the tumor. Conversely, consider the inverse problem of matching the image without the tumor to the one with the tumor. A valid registration in this case may be to register all of the corresponding brain structures by allowing the transformation to "tear" (i.e., not be diffeomorphic) at the site of the tumor. Just as valid could be a diffeomorphic transformation that registers all of the corresponding brain structures by allowing the transformation to stretch at the site of the tumor.

As in the previous examples, we will assume that a valid transformation is diffeomorphic everywhere except possibly in regions where the source and target images differ topologically, e.g., in the neighborhood of the tumor. For the remainder of the this paper, we will consider registration problems that the diffeomorphic transformation assumption is valid. These ideas can be extended to certain non-diffeomorphic mapping problems by including boundary conditions to model, isolate or remove regions that differ topologically.

Transformations that are diffeomorphic maintain topology guaranteeing that connected subregions remain connected, neighborhood relationships between structures are preserved, and surfaces are mapped to surfaces. Preserving topology is important for synthesizing individualized electronic atlases; the knowledge base of the atlas maybe transferred to the target anatomy through the topology preserving transformation providing automatic labeling and segmentation. If total volume of a nucleus, ventricle, or cortical sub region are an important statistic it can be generated automatically. Topology preserving transformations that map the template to the target also can be used to study the physical properties of the target anatomy such as mean shape and variation. Likewise, preserving topology allows data from multiple individuals to be mapped to a standard atlas coordinate space [1]. Registration to an atlas removes individual anatomical variation and allows information from many experiments to be combined and associated with a single conical anatomy.

The forward transformation h from image T to S and the reverse transformation g from S to T are pictured in Fig. 1. Ideally, the transformations h and g should be uniquely determined and should be inverses of one another. Estimating h and g independently very rarely results in a consistent set of transformations due to a large number of local minima. As a result, we propose to jointly estimate h and g while constraining these transforms to be inverses of one another. The joint estimation makes intuitive sense in that the invertibility constraint will reduce the number of local minima because the problem is being solved

from two different directions. Although uniqueness is very difficult to achieve in medical image registration, the joint estimation should lead to more consistent and biologically meaningful results.

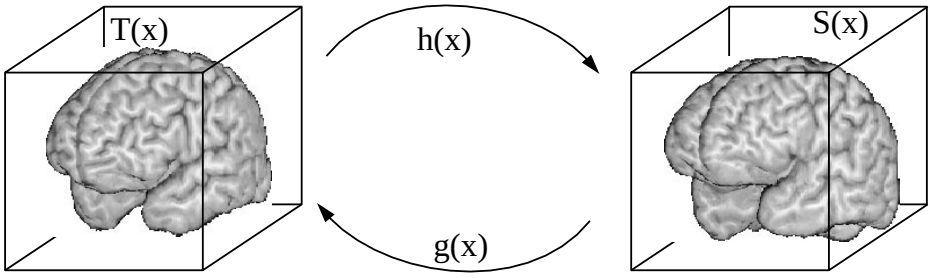

Fig. 1. The transformation h maps the image volume T to S and the transformation g maps S to T. In order for the mappings to be biologically meaningful, h and g should be inverses of one another

The need to impose the invertibility consistency constraint depends on the particular application and on the correspondence model used for registration. In general, registration techniques that do not uniquely determine the correspondence between image volumes should benefit from the consistency constraint. This is because such techniques often rely on minimizing/maximizing a similarity measure which has a large number of local minima/maxima due to correspondence ambiguity. Examples include similarity measures based on features in the source and target images such as image intensities, object boundaries/surfaces, etc. In theory, similarity measures have more local minima as the dimension of the transformation increases. A registration method that determines the correspondence between images by minimizing an image intensity similarity measure is considered in this paper.

Methods that use specified correspondences for registration will benefit less or not at all from the invertibility consistency constraint. For example, landmark based registration methods implicitly impose an invertibility constraint because the correspondence defined between landmarks is the same for estimating the forward and inverse transformations. However, the drawbacks of specifying correspondences include requiring user interaction to specify landmarks, unique correspondences can not always be specified, and such methods usually only provide coarse registration due to the small number of correspondences specified.

2 Registration Algorithm

2.1 Problem Statement

The image registration problem is usually stated as: Find the transformation h that maps the template image volume T into correspondence with the target

image volume S. Alternatively, the problem can be stated as: Find the transformation g that transforms S into correspondence with T. For this paper, the previous two statements are combined into a single problem and restated as:

> **Problem Statement:** Jointly estimate the transformations h and g such that h maps T to S and g maps S to T subject to the constraint that $h = g^{-1}$.

It is assumed that the 3D image volumes T and S are medical imaging modalities such as MRI, fMRI, CT, cryosection imagery, etc. collected from similar anatomical populations. Each image is defined as a function of $x \in \Omega = [0,1]^3$ where Ω is called the image coordinate system. The transformations are vector-valued functions that map the image coordinate system Ω to itself, i.e., $h : \Omega \mapsto \Omega$ and $g : \Omega \mapsto \Omega$. Diffeomorphic constraints are placed on h and g so that they preserve topology. Throughout it is assumed that $h(x) = x + u(x)$, $h^{-1}(x) = x + \tilde{u}(x)$, $g(x) = x + w(x)$ and $g^{-1}(x) = x + \tilde{w}(x)$ where $h(h^{-1}(x)) = x$ and $g(g^{-1}(x)) = x$. All of the fields h, g, u, $\tilde{u}$, w, and $\tilde{w}$ are (3×1) vector-valued functions of $x \in \Omega$.

Registration is defined using a symmetric cost function $C(h, g)$ that describes the distance between the transformed template $T(h)$ and target S, and the distance between the transformed target $S(g)$ and template T. To ensure the desired properties, the transformations h and g are jointly estimated by minimizing the cost function $C(h, g)$ while satisfying diffeomorphic constraints and inverse transformation consistency constraints. The diffeomorphic constraints are enforced by constraining the transformations to satisfy laws of continuum mechanics [2].

2.2 Symmetric Cost Function

The main problem with image similarity registration techniques is that minimizing the similarity function does not uniquely determine the correspondence between two image volumes. In addition, similarity cost functions generally have many local minima due to the complexity of the images being matched and the dimensionality of the transformation. It is these local minima (ambiguities) that cause the estimated transformation from image T to S to be different from the inverse of the estimated transformation from S to T. In general, this becomes more of a problem as the dimensionality of the transformation increases. To overcome this problem for 3×3 linear transformations, Woods et al. [3] averages the forward and inverse linear transformations to reconcile differences between pairwise registrations.

To overcome correspondence ambiguities, we jointly estimate the transformations from image T to S and from S to T. This is accomplished by defining a cost function to measure the shape differences between the deformed image $T(h(x))$ and image $S(x)$ and the differences between the deformed image $S(g(x))$ and image $T(x)$. Ideally, the transformations h and g should be inverses of one another, i.e., $h(x) = g^{-1}(x)$. The transformations h and g are estimated by minimizing a cost function that is a function of $(T(h(x)) - S(x))$ and $(S(g(x)) - T(x)$. The

cost function used in this work is given by

$$C_1(T(h),S)+C_1(S(g),T)=\int_\Omega |T(h(x))-S(x)|^2dx+\int_\Omega |S(g(x))-T(x)|^2dx. \tag{1}$$

Alternatively, the mutual information cost function given in [4,5] could be used. Notice that this joint estimation approach applies to both linear and non-linear transformations.

2.3 Transformation Parameterization

A 3D Fourier series representation is used to parameterize the forward and inverse transformations. This parameterization is simpler than the parameterizations used in our previous work [6,7,8] and each basis coefficient can be interpreted as the weight of a harmonic component in a single coordinate direction. The displacement fields are constrained to have the form

$$u(x)=\sum_{k=0}^{N-1}\sum_{j=0}^{N-1}\sum_{i=0}^{N-1}\mu_{ijk}e^{\hat{j}<x,\omega_{ijk}>} \quad \text{and} \quad w(x)=\sum_{k=0}^{N-1}\sum_{j=0}^{N-1}\sum_{i=0}^{N-1}\eta_{ijk}e^{\hat{j}<x,\omega_{ijk}>} \tag{2}$$

where μ_{ijk} and η_{ijk} are (3×1), complex-valued vectors and $\omega_{ijk}=[\frac{2\pi i}{N},\frac{2\pi j}{N},\frac{2\pi k}{N}]$. Notice that this parameterization is periodic in x and therefore has cyclic boundary conditions for x on the boundary of Ω . The coefficients μ_{ijk} and η_{ijk} are constrained to have complex conjugate symmetry during the estimation procedure.

Proposition 1. *Each displacement field in (2) is real and can be written as*

$$u(x)=2\sum_{k=0}^{N-1}\sum_{j=0}^{N-1}\sum_{i=0}^{N/2-1}\left(a_{ijk}Re\{e^{\hat{j}<x,\omega_{ijk}>}\}-b_{ijk}Im\{e^{\hat{j}<x,\omega_{ijk}>}\}\right) \tag{3}$$

if the (3×1) *vector* $\mu_{ijk}=a_{ijk}+\hat{j}b_{ijk}$ *has complex conjugate symmetry.*

Proof. Notice that (2) can be written as

$$u(x)=\sum_{k=0}^{N-1}\sum_{j=0}^{N-1}\sum_{i=0}^{N/2-1}(a_{ijk}+\hat{j}b_{ijk})e^{\hat{j}<x,\omega_{ijk}>}+(a_{ijk}-\hat{j}b_{ijk})e^{-\hat{j}<x,\omega_{ijk}>}$$

because the μ_{ijk} are complex conjugate symmetric. Simplifying the summand gives the result. □

2.4 Inverse Transformation Consistency Constraint

Minimizing the cost function in (1) is not sufficient to guarantee that the transformations h and g are inverses of each other. The inverse transformation consistency constraint is enforced by minimizing the squared difference between the transformation h and and the inverse transformation of g, and vice versa. To state this mathematically we define the following relationships: $h(x) = x + u(x)$, $h^{-1}(x) = x + \tilde{u}(x)$, $g(x) = x + w(x)$ and $g^{-1}(x) = x + \tilde{w}(x)$. The consistency constraint is enforced by minimizing

$$C_2(u, \tilde{w}) + C_2(w, \tilde{u}) = \int_\Omega ||u(x) - \tilde{w}(x)||^2 dx + \int_\Omega ||w(x) - \tilde{u}(x)||^2 dx. \quad (4)$$

The inverse transformation h^{-1} is estimated from h by solving the minimization problem $h^{-1}(y) = \arg\min_x ||y - h(x)||^2$ for each y on a discrete lattice in Ω. The inverse h^{-1} exists and is unique if h is a diffeomorphic transformation, i.e., continuous, one-to-one, and onto.

2.5 Diffeomorphic Constraint

Minimizing the cost function in (4) does not ensure that the transformations h and g are diffeomorphic transformations except for when $C_2(u, \tilde{w}) + C_2(w, \tilde{u}) = 0$. To enforce the transformations to be diffeomorphic, we use continuum mechanical models such as linear elasticity [7,9] and viscous fluid [9,10]. For this paper, a linear-elastic constraint of the form

$$C_3(u) + C_3(w) = \int_\Omega ||Lu(x)||^2 dx + \int_\Omega ||Lw(x)||^2 dx \quad (5)$$

was used to enforce the diffeomorphic property where $h(x) = x + u(x)$ and $g(x) = x + w(x)$. The operator L has the form $Lu(x) = -\alpha\nabla^2 u(x) - \beta\nabla(\nabla \cdot u(x)) + \gamma$ for linear elasticity, but in general can be any nonsingular linear differential operator [8].

Following the approach in [8], the operator L can be considered a (3×3) matrix operator. Discretizing the continuous partial derivatives of L, it can be shown that (5) has the form

$$C_3(u) + C_3(w) = N^3 \sum_{k=0}^{N-1} \sum_{j=0}^{N-1} \sum_{i=0}^{N-1} \mu_{ijk}^\dagger D_{ijk}^2 \mu_{ijk} + \eta_{ijk}^\dagger D_{ijk}^2 \eta_{ijk} \quad (6)$$

where † is the complex conjugate transpose. D_{ijk} is a real-valued, (3×3) matrix with elements

$$d_{11} = 2\alpha\Big[\beta\Big(1 - \cos\Big(\tfrac{2\pi i}{N}\Big)\Big) + \Big(1 - \cos\Big(\tfrac{2\pi j}{N}\Big)\Big) + \Big(1 - \cos\Big(\tfrac{2\pi k}{N}\Big)\Big)\Big] + \gamma$$

$$d_{22} = 2\alpha\Big[\Big(1 - \cos\Big(\tfrac{2\pi i}{N}\Big)\Big) + \beta\Big(1 - \cos\Big(\tfrac{2\pi j}{N}\Big)\Big) + \Big(1 - \cos\Big(\tfrac{2\pi k}{N}\Big)\Big)\Big] + \gamma$$

$$d_{33} = 2\alpha\Big[\Big(1-\cos\Big(\tfrac{2\pi i}{N}\Big)\Big)+\Big(1-\cos\Big(\tfrac{2\pi j}{N}\Big)\Big)+\beta\Big(1-\cos\Big(\tfrac{2\pi k}{N}\Big)\Big)\Big]+\gamma$$
$$d_{12} = d_{21} = \beta\Big[\cos\Big(\tfrac{2\pi}{N}(i-j)\Big)-\cos\Big(\tfrac{2\pi}{N}(i+j)\Big)\Big]$$
$$d_{13} = d_{31} = \beta\Big[\cos\Big(\tfrac{2\pi}{N}(i-k)\Big)-\cos\Big(\tfrac{2\pi}{N}(i+k)\Big)\Big]$$
$$d_{23} = d_{32} = \beta\Big[\cos\Big(\tfrac{2\pi}{N}(j-k)\Big)-\cos\Big(\tfrac{2\pi}{N}(j+k)\Big)\Big].$$

2.6 Minimization Problem

By combining (1), (4), and (5), the image registration problem becomes

$$\begin{aligned}\hat{h}(x),\hat{g}(x) = \underset{h(x),g(x)}{\arg\min}\int_{\Omega}|T(h(x))-S(x)|^2+|S(g(x))-T(x)|^2dx\\ +\lambda\int_{\Omega}||u(x)-\tilde{w}(x)||^2+||w(x)-\tilde{u}(x)||^2dx\\ +\rho\int_{\Omega}||Lu(x)||^2+||Lw(x)||^2dx\end{aligned} \tag{7}$$

where the constants λ and ρ are Lagrange multipliers used to enforce/balance the constraints.

2.7 Estimation Procedure

The transformations $\hat{h}$ and $\hat{g}$ that satisfy (7) were estimated using a gradient descent algorithm to determine the basis coefficients $\{\mu_{ijk}, \eta_{ijk}\}$. The estimation was accomplished by solving a sequence of optimization problems from coarse to fine scale via increasing the number of the basis coefficient vectors $\{\mu_{ijk}, \eta_{ijk}\}$ during the estimation. This is analogous to multi-grid methods but here the notion of refinement from coarse to fine is accomplished by increasing the number of basis components. As the number of basis functions is increased, smaller and smaller variabilities between the template and target images are accommodated.

3 Results

Two MRI and two CT image volumes were used to evaluate the registration algorithm. The data sets were collected from different individuals using the same MR and CT machines and the same scan parameters. The MRI data sets correspond to two normal adults and the CT data sets correspond to two 3-month-old infants, one normal and one abnormal (bilateral coronal synostosis). The MRI and CT data sets were chosen to test registration algorithm when matching anatomies with similar and dissimilar shapes, respectively.

The MRI data were preprocessed by normalizing the image intensities, correcting for translation and rotation, and segmenting the brain from the head

using Analyze^{TM}. The translation aligned the anterior commissure points, and the rotation aligned the corresponding axial and sagittal planes containing the anterior and posterior commissure points, respectively. The data sets were then down-sampled and zero padded to form a $64 \times 64 \times 64$ voxel lattice. The CT data sets were corrected for translation and rotation and down-sampled to form a $64 \times 64 \times 50$ voxel lattice. The translation aligned the basion skull landmarks, and the rotation aligned the corresponding Frankfort Horizontal and midsagittal planes, respectively.

The data sets were registered initially with zero and first order harmonics. After every 40th iteration, the maximum harmonic was increased by one. The MRI-to-MRI registration was terminated after 300 iterations and the CT-to-CT registration was terminated after 200 iterations. Tables 1, 2, and 3 show the results of four MRI experiments and four CT experiments. In order to isolate the contribution of each term of (7), one experiment was done with no priors, one with the linear-elastic model, one with the inverse consistency constraint, and one with both priors. The four MRI experiments used the parameters 1. $\lambda = \rho = 0$, 2. $\lambda = 0$ and $\rho = 50$, 3. $\lambda = 0.07$ and $\rho = 0$, and 4. $\lambda = 0.07$ and $\rho = 50$; and four CT experiments used the parameters: 1. $\lambda = \rho = 0$, 2. $\lambda = 0$ and $\rho = 25$, 3. $\lambda = 0.02$ and $\rho = 0$, and 4. $\lambda = 0.02$ and $\rho = 25$. The labels MRI1 and CT1 are used to refer to results from the Case 1 experiments, and likewise for 2 to 4.

Table 1. Cost Terms Associated with Transforming Image Volume T to S

Experiment	$C_1(T(h), S)$		$\lambda C_2(u, \tilde{w})$	$\rho C_3(u)$	Total
	orig.	final	final	final	
MRI1	1980	438	0	0	438
MRI2	1980	606	0	85.7	692
MRI3	1980	482	33.4	0	516
MRI4	1980	639	13.0	74.6	727
CT1	454	27.0	0	0	27.0
CT2	454	38.8	0	28.1	66.9
CT3	454	28.5	3.15	0	31.6
CT4	454	40.8	3.34	28.3	72.4

Case 1. corresponds to unconstrained estimation in which h and g are estimated independently. The numbers in the tables are consistent with this observation. First, $C_2(u, \tilde{w})$ and $C_2(w, \tilde{u})$ show the largest error between the forward and inverse mapping for each group of experiments. Secondly, the Jacobian for these cases are the lowest in their respective groups. This is expected because the unconstrained experiments find the best match between the images without any constraint preventing the Jacobian from going negative (singular). This is further supported by the fact that the final values of $C_1(T(h), S)$ and $C_1(S(g), T)$ are the lowest in there groups.

Table 2. Cost Terms Associated with Transforming Image Volume S to T

Experiment	$C_1(S(g),T)$		$\lambda C_2(w,\tilde{u})$	$\rho C_3(w)$	Total
	orig.	final	final	final	
MRI1	1980	512	0	0	512
MRI2	1980	660	0	78.3	738
MRI3	1980	539	33.6	0	573
MRI4	1980	676	13.0	73.7	727
CT1	454	30.6	0	0	30.6
CT2	454	47.7	0	32.4	80.1
CT3	454	34.6	3.43	0	38.0
CT4	454	50.8	3.78	31.9	86.5

Case 2. corresponds to independently estimating h and g while requiring each transformation to satisfy the diffeomorphic constraint enforced by linear elasticity. Just as in Case 1, the large difference between the forward and reverse displacement fields as reported by $C_2(u,\tilde{w})$ and $C_2(w,\tilde{u})$ confirms that linear elasticity alone is not sufficient to guarantee that h and g are inverses of one another. We do however, see that the linear elasticity constraint did improve the transformation over the unconstrained case because the minimum Jacobian and the inverse of the maximum Jacobian is far from being singular.

Case 3. corresponds to the estimation problem that is constrained only by the inverse transformation consistency constraint. The $C_2(u,\tilde{w})$ and $C_2(w,\tilde{u})$ values for these experiments are much lower than those in Cases 1. and 2. because they are being minimized. The transformations h and g are inverses of each other when $C_2(u,\tilde{w}) + C_2(w,\tilde{u}) = 0$ so that the smaller the costs $C_2(u,\tilde{w})$ and $C_2(w,\tilde{u})$ are, the closer h and g are to being inverses of each other.

Table 3. Transformation Measurements

Experiment	Jacobian(h)		Jacobian(g)		$C_2(u,\tilde{w})$	$C_2(w,\tilde{u})$
	min	1/max	min	1/max		
MRI1	0.257	0.275	0.100	0.261	28,300	29,500
MRI2	0.521	0.459	0.371	0.653	10,505	10,460
MRI3	0.315	0.290	0.226	0.464	478	479
MRI4	0.607	0.490	0.410	0.640	186	186
CT1	0.340	0.325	0.200	0.49	73,100	76,400
CT2	0.552	0.490	0.421	0.678	28,700	28,300
CT3	0.581	0.361	0.356	0.612	158	171
CT4	0.720	0.501	0.488	0.725	167	189

Case 4. is the joint estimation of h and g with both the inverse consistency constraint and the linear-elastic constraint. We can see that this produced the

best results because the differences between the inverse transformations were so small, i.e., $C_2(u, \tilde{w})$ and $C_2(w, \tilde{u})$. Also, the minimum Jacobian of h is nearly the inverse of the maximum Jacobian of g, and vice versa. In addition, the minimum and one over the maximum Jacobian of h and g have their largest values for this experiment (excluding one entry from MRI2). The MRI4 experiment shows a better than twofold improvement over MRI3 with respect to the difference in the inverse transformations, while the the inverse transformations difference for the CT4 and CT3 experiments are nearly equal. This may suggest that the inverse consistency constraint may be used without the linear-elasticity constraint. However, the minimum and one over the maximum Jacobian values are larger for CT4 than CT3 and similarly for MRI4 and MRI3 suggesting less distortion. The closer the minimum Jacobian is to one, the smaller the distortion of the images.

Figure 2 shows three slices from the 3D result of Case 4 for both the MRI and CT experiments. The first two columns show the template T and target S images before transformation. The third and forth columns show the transformed template $T(h)$ and target $S(g)$. Columns 5,6, and 7 show the x-,y-, and z-components of the displacement field u used to deform the template and columns 8,9, and 10 show the same for the displacement field w. The near invertibility in gray-scale between the displacement fields u and w gives a visual impression that h and g are nearly inverses of each other.

The time series statistics for MRI4 and CT4 experiments are shown in Figs. 3 and 4. These graphs show that the gradient descent algorithm converged for each set of transformation harmonics. In both cases, the cost functions $C_1(T(h), S)$ and $C_1(S(g), T)$ decreased at each iteration while the prior terms increased before decreasing. Notice that the inverse consistency constraint increased as the images deformed for each particular harmonic resolution. Then when the number of harmonics were increased, the inverse constraint decreased before increasing again. This is due to the fact that a low-dimensional Fourier series does not have enough degrees of freedom to faithfully represent the inverse of a low-dimensional Fourier series. This is easily seen by looking at the high dimensionality of a Taylor series representation of the inverse transformation. Finally, notice that the inverse consistency constraint caused the extremal Jacobian values of the forward and reverse transformations to track together. This is easiest to see in the CT4 experiment. Note that these extremal Jacobian values correspond to the worst case distortions produced by the transformations.

4 Discussion

The experiments presented in this paper were designed to test the validity of the new inverse transformation consistency constraint as applied to a linear-elastic transformation algorithm. As such, there was no effort made to optimize the rate of convergence of the algorithm. The convergence rate of the algorithm can be greatly improved by using a more efficient optimization technique than gradient descent such as conjugate gradient at each parameterization resolution. In

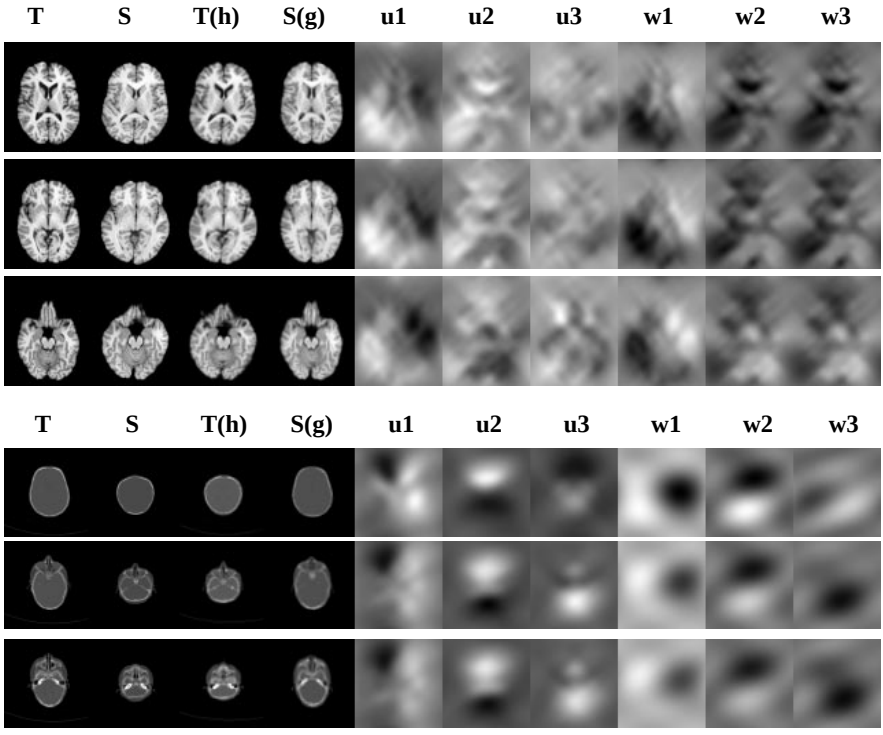

Fig. 2. Images associated with the MRI4 and CT4 experiments

addition, a convergence criteria can be used to determine when to increment the number of parameters in the model. The CT data used in the experiments was selected to stress the registration algorithm. The convergence of the algorithm would have been much faster if the data sets were adjusted for global scale initially.

It is important to track both the minimum and maximum values of the Jacobian during the estimation procedure. The Jacobian measures the differential volume change of a point being mapped through the transformation. At the start of the estimation, the transformation is the identity mapping and therefore has a Jacobian of one. If the minimum Jacobian goes negative, the transformation is no longer a one-to-one mapping and as a result folds the domain inside out [11]. Conversely, the reciprocal of the maximum value of the Jacobian corresponds to the minimum value of the Jacobian of the inverse mapping. Thus, as the maximum value of the Jacobian goes to infinity, the minimum value of the Jacobian of the inverse mapping goes to zero. In the present approach, the inverse transformation consistency constraint was used to penalize transformations that deviated from their inverse transformation. A limitation of this approach is that cost function in (4) is an average metric and can not enforce the pointwise constraints that $\min_x\{J(h)\} = 1/\max_x\{J(g)\}$ and $\min_x\{J(g)\} = 1/\max_x\{J(h)\}$. This

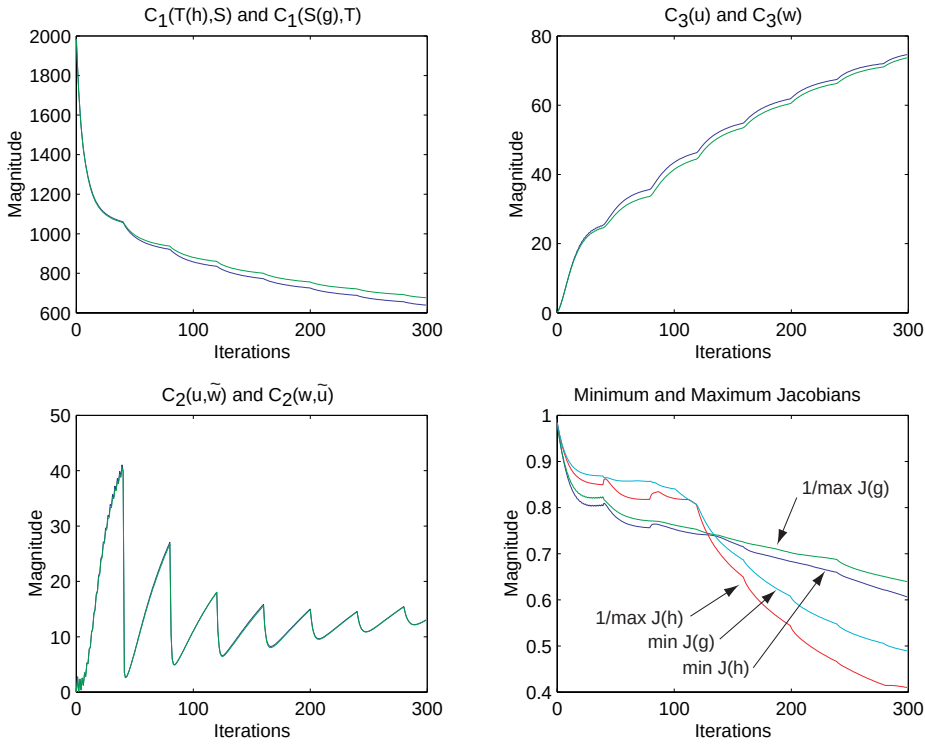

Fig. 3. Statistics associated with the MRI4 experiment

point is illustrated by Table 3 by the fact that the minimum values of $J(h)$ and $J(g)$ differ from the reciprocal of the maximum values of $J(g)$ and $J(h)$, respectively, However, these extremal Jacobian values do give an upper-bound on the worst case distortions produced by the transformations demonstrating the consistency between the forward and reverse transformations.

5 Summary and Conclusions

This paper presented a new algorithm for jointly estimating a consistent set of transformations that map one image to another and vice versa. A new parameterization based on the Fourier series was presented and was used to simplify the discretized linear-elasticity constraint. The Fourier series parameterization is simpler than our previous parameterizations and each basis coefficient can be interpreted as the weight of a harmonic component in a single coordinate direction. The algorithm was tested on both MRI and CT data. It was found that the unconstrained estimation leads to singular or near transformations. It was also shown that the linear-elastic constraint alone is not sufficient to guarantee that the forward and reverse transformations are inverses of one another. Results

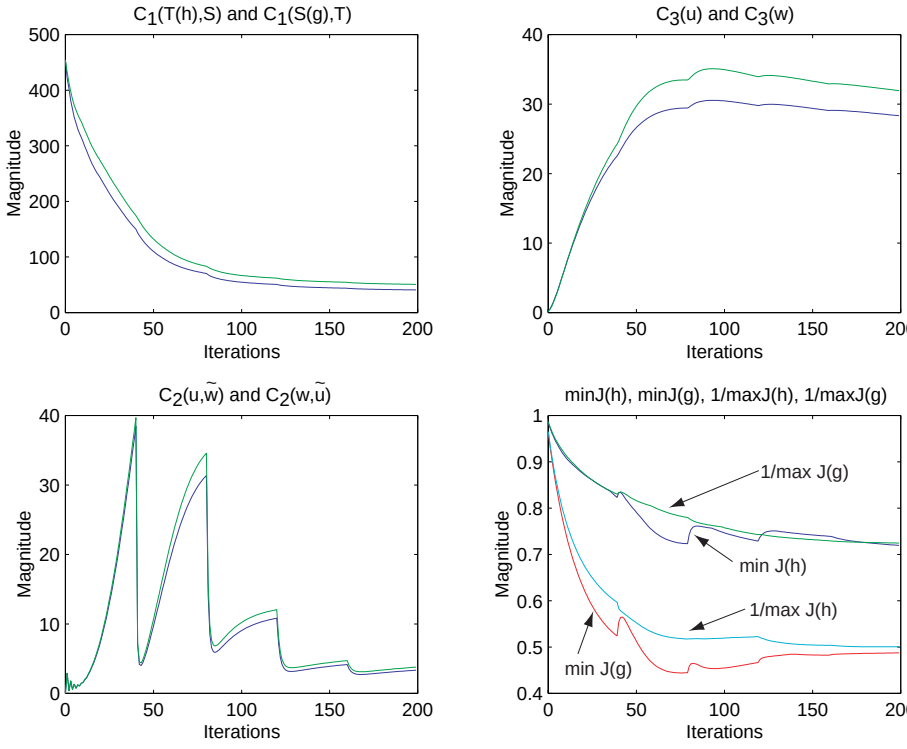

Fig. 4. Statistics associated with the CT4 experiment

were presented that suggest that even thought the inverse consistency constraint is not guaranteed to generate nonsingular transformations, in practice it may be possible to use the inverse consistency as the only constraint. Finally, it was shown that the most consistent transformations were generated using both the inverse consistency and the linear-elastic constraints.

Acknowledgments

I would like to thank my graduate students Hans Johnson and Peng Yin for their help in preparing this manuscript. I would like to thank John Haller and Michael W. Vannier of the Department of Radiology, The University of Iowa for providing the MRI data. I would like to thank Jeffrey L. Marsh of the Department of Surgery, Washington University School of Medicine for providing the CT data. I would like to thank Michael I. Miller and Sarang C. Joshi for their helpful insights over the last eight plus years. This work was supported in part by the NIH grant NS35368 and a grant from the Whitaker Foundation.

References

1. Talairach, J., Tournoux, P.: Co-Planar Stereotactic Atlas of the Human Brain. Beorg Thieme Verlag, Stuttgart, 1988
2. Segel, L.A.: Mathematics Applied to Continuum Mechanics. Dover Publications, New York, 1987
3. Woods, R.P., Grafton, S.T., Watson, J.D., Sicotte, N.L., Mazziotta, J.C.: Automated Image Registration: II. Intersubject Validation of Linear and Nonlinear Models. Journal of Computer Assisted Tomography **22** (1998) 153–165
4. Maes, F., Collignon, A., Vandermeulen, D., Marchal, G., Suetens, P.: Multimodality image registration by maximization of mutual information. IEEE Transactions on Medical Imaging **16** (1997) 187–198
5. Wells III, W.M., P.Viola, P., Atsumi, H., Nakajima, S., Kikinis R.: Multi-modal volume registration by maximization of mutual information. Medical Image Analysis **1** (1996) 35–51
6. Miller, M.I., Christensen, G.E., Amit, Y., Grenander, U.: Mathematical textbook of deformable neuroanatomies. Proceedings of the National Academy of Sciences **90** (1993) 11944–48
7. Christensen, G.E., Rabbitt, R.D., Miller, M.I.: 3D brain mapping using a deformable neuroanatomy. Physics in Medicine and Biology **39** (1994) 609–618
8. Miller, M.I., Banerjee, A., Christensen, G.E., Joshi, S.C., Khaneja, N., Grenander, U., Matejic, L.: Statistical methods in computational anatomy. Statistical Methods in Medical Research **6** (1997) 267–299
9. Christensen, G.E., Joshi, S.C., Miller, M.I.: Volume geometric transformations for mapping anatomy. IEEE Trans. on Med. Imaging **16** (1997) 864–877
10. Christensen, G.E., Rabbitt, R.D., Miller, M.I.: Deformable templates using large deformation kinematics. IEEE Transactions on Image Processing **5** (1996) 1435–1447
11. Christensen, G.E., Rabbitt, R.D., Miller, M.I., Joshi, S.C.,, Grenander, U., Coogan, T.A., Van Essen, D.C.: Topological properties of smooth anatomic maps. In Bizais, Y., Braillot, C., Di Paola, R.. editors, Information Processing in Medical Imaging, Kluwer Academic Publishers, Boston (1995) 101–112